12^{th} International Conference on Fracture Mechanics of Concrete and Concrete Structures
FraMCoS-12
B.L.A. Pichler, Ch. Hellmich, P. Preinstorfer (Eds)

https://doi.org/10.21012/FC12.1250
TT-C1:3

NUMERICAL ANALYSIS OF SIZE-EFFECT IN UHPFRC BEAMS IN PURE BENDING WITH FOCUS ON TRANSITION FROM SINGLE TO MULTIPLE CRACKING

JAIME PLANAS*, BEATRIZ SANZ† AND JOSE M. SANCHO‡

Universidad Politécnica de Madrid, CIME (Centro de Investigación en Materiales Estructurales)
Profesor Aranguren 3, 28039 Madrid, Spain.
e-mail: * jaime.planas@upm.es , †beatriz.sanz@upm.es , ‡jose.sancho@upm.es

Key words: Cohesive Crack, Multiple Cracking, Fibre-Bridging, Size-Effect, UHPFRC

Abstract. Ultra-high performance fibre reinforced concrete (UHPFRC) emerged in the last two decades as a technologically sound building material. It is well known that, in direct tension, softening takes place for an UHPFRC as long as its fibre content is relatively small. However, strong hardening may still be obtained for such a material in bending with, possibly, concurrent stable, multiple cracking. Yet, the ability to harden under bending is not a material property, but a mixed material-structural property, and thus subjected, very particularly, to size-effect, where the expression size-effect is used in this context in its widest sense of the influence of size on all the aspects characterizing the mechanical response, such as the full load-displacement curve and the whole evolution of the crack pattern. In this paper, some basic results of a wider numerical study of size- and material-effect are reported for softening UHPFRCs characterized by a steep initial softening due to matrix cracking followed by a long, slow softening due to fibre-bridging. The simulations were devised to investigate the coupled influence of the initial softening slope and of the fibre bridging stresses on the response of similar beams in pure bending, and cracking was simulated using finite elements with embedded cohesive cracks (in Hillerborg's sense). The results show that the nominal stress at visible crack initiation depends essentially on the sharp initial softening and specimen size, while the intensity of post-crack hardening and mean crack spacing (as well as mean crack opening) depend on the fibre bridging strength and the specimen size. Dimensionless plots are provided that allow utilization of the results for other combinations of data in the domain of the simulations.

1 INTRODUCTION

This work aroused in the frame of a research aimed at developing sound experimental techniques to characterize the fracture properties of ultra-high performance fibre reinforced concrete (UHPFRC), a modern and technologically mature product, with specific official recommendations and norms (see, e.g. [1–3]), but still lacking a full support for fracture mechanics characterization. A first glimpse into the subject of multiple cracking in bending of beams of UHPFRC was recently given in [4] —following previous trends developed in [5, 6]— of which the present paper is an extension.

As pointed out in [4], UHPFRC is, essentially, a composite made of an ultra high performance cement mortar —the matrix— reinforced with fibers (most commonly, high strength steel fibers). Although much stronger than ordinary and high strength mortars, such matrix still behaves as a quasibrittle material that fails in tension with little plastic strain. The progressive addition of fibers increases the toughness of the material, due to their crack-

bridging effect, until the material starts displaying a plastic-like behavior, which means that inelastic distributed strains are produced under increasing load before softening starts.

However, for relatively small fibre content, softening still occurs in pure tension although strong hardening may be seen in bending [7]; this effect is used in the recommendations to classify the tensile performance of a particular concrete as belonging to one of three categories: (1) the specimens fails through a single crack, both for direct tension and bending, with small inelastic deformations prior to the peak load; (2) for pure tension the specimens fail through a single crack and negligible inelastic deformations prior to the peak load, but relatively large inelastic deformations and hardening before the peak is reached in specimens tested in bending; and (3) both in pure tension and bending a relatively large inelastic deformation with hardening occurs prior to the peak load.

Focussing on the behavior displayed by categories (1) and (2), in which the cracking is generally described by a cohesive crack model in the sense of Hillerborg [8–12], it may be expected that the strength, the hardening behavior and the crack pattern in bending all depend on the size of the specimen. This was indeed found experimentally in [13], and the main objective of this and the previous paper [4] is to set the ground for a systematic numerical analysis of the size effect in the bending tests of materials that display a behavior in pure tension resembling that of a UHPFRC in categories (1) and (2). In this paper we analyze in more detail new extreme cases that were not dealt with previously, and which can led to a better understanding of the overall size-effect trends when approaching the small size limit.

The paper is organized as follows: in Sec. 2, the background necessary to understand the rest of the paper is presented ; in Sec. 3, the material behavior, the geometry and the meshes used in the computations are described; in Sec. 4, the results are presented and discussed; Sec. 5 closes with some final remarks.

2 BACKGROUND

In the analysis presented next, cracking of a quasibrittle material such as concrete or non-hardening UHFRC is modeled using a generalization of the cohesive crack in the sense of Hillerborg [8–12]. For pure opening (Mode I), the crack forms perpendicular to the maximum principal stress and the stress σ transferred across its faces is a unique function of the crack separation w:

$$\sigma = f(w) \ . \tag{1}$$

The material function $f(w)$ is usually called the softening curve or softening function and is the main ingredient of the model.

For general loading, a *vectorial* traction-separation law is required between the traction vector $\mathbf{t}$ acting on on one of the faces of the crack (which is taken as the reference face) and the crack separation vector $\mathbf{w}$. A quite general damage-based vectorial model was recently proposed by the authors in [14] and summarily expounded in [4]. However, since in the present problem the cracks open primarily in pure Mode I, we actually use the simplest of the available models as described, for example, in [15], in which $\mathbf{t}$ and $\mathbf{w}$ are parallel (so called central force model) and the crack evolution is governed by a never decreasing damage variable κ so that the equations for the crack are

$$\mathbf{t} = \frac{f(\kappa)}{\kappa}\mathbf{w} \ , \qquad \kappa = \max[|\mathbf{w}|], \tag{2}$$

where $f(\cdot)$ is the Mode I softening function introduced in Eq (1). Note that for pure opening mode $\mathbf{w} = w\mathbf{n}$ and $|\mathbf{w}| = w$ (with $\mathbf{n} =$ unit normal to the crack). If, furthermore, w increases monotonically, then $\kappa = w$ and $\mathbf{t} = \sigma\mathbf{n} = f(w)\mathbf{n}$ and, thus, Hillerborg's uniaxial model is recovered.

To carry out the analysis of the size-effect, the first step is to use a dimensionless version of the softening curve (1) by selecting a characteristic cohesive stress σ_{ch} and a characteristic crack opening w_{ch} to write the softening function in the dimensionless form

$$\sigma = f(w) = \sigma_{\text{ch}}\hat{f}\left(\frac{w}{w_{\text{ch}}}\right) \ . \tag{3}$$

If, next, one considers geometrically similar specimens (or structures) made of a crackable linear elastic material subjected to proportional loading and gets a mechanically valid solution for one particular structure 'A' of size D^A (beam depth, say), made of an elastic material with an elastic modulus E^A, having a particular cohesive crack pattern satisfying equations (2) with a softening function given by (3) with particular characteristic values σ_{ch}^A and w_{ch}^A, then it turns out that another geometrically similar structure will accept a mechanically valid solution similar to that for structure A as long as the combination of its size D and material properties E, σ_{ch} and w_{ch} satisfies the condition

$$\frac{Ew_{\text{ch}}}{D\sigma_{\text{ch}}} = \frac{E^A w_{\text{ch}}^A}{D^A \sigma_{\text{ch}}^A} \quad \text{or} \quad \frac{\ell^*}{D} = \frac{\ell_A^*}{D^A} \,, \tag{4}$$

$$\text{with} \quad \ell^* := \frac{Ew_{\text{ch}}}{\sigma_{\text{ch}}}. \tag{5}$$

When this is the case, the stress and displacement fields in the similar structure (at homologous points) satisfy the similarity rules

$$\frac{\boldsymbol{\sigma}}{\sigma_{\text{ch}}} = \frac{\boldsymbol{\sigma}^A}{\sigma_{\text{ch}}^A} \,, \qquad \frac{\mathbf{u}}{w_{\text{ch}}} = \frac{\mathbf{u}^A}{w_{\text{ch}}^A} \tag{6}$$

and likewise for the crack tractions and separations. Note that these rules are valid with the implicit conditions that the value of Poisson's ratio and the shape of the softening curve of the two materials be the same.

The mixed parameter ℓ^* in $(5)_3$ is a characteristic length which precise expression depends on the choice of the characteristic values: while $\sigma_{\text{ch}} := f_t$ seems to be a universal choice, various choices are possible for w_{ch}. If one takes $w_{\text{ch}} = G_F/f_t$ the result for ℓ^* is Hillerborg's characteristic length. Here we take $w_{\text{ch}} = w_1 =$ initial subtangent of the softening curve as shown in Fig. 2 to get the *second characteristic length*, which reads [6]

$$\ell_2 := \frac{Ew_1}{f_t} \,. \tag{7}$$

Thus, according to Eq. (4) geometrically similar structures will be also mechanically similar if their value of ℓ_2/D is the same, and, since in most if not all cases, the strength of a quasibrittle structure increases with increasing ℓ_2/D, it would be appropriate to call it something like *structural toughness number*.

3 NUMERICAL SIMULATIONS

In this work we consider the same type of beams and meshes as in [4] as depicted in Fig 1. The central loading span S is taken to be seven times the beam depth to allow for the development of multiple cracks in cases of hardening. Two meshes have been used for the calculations which are also shown in Fig 1. The meshes were created using the program GMSH [16], with the meshing algorithm set to "Delaunay" and applying smoothing.

In this work, as in [4], the material is modeled as quasibrittle linear elastic with Poisson's ratio $\nu = 0.17$ and bilinear cohesive fracture characterized by the four parameters f_t, w_1, f_1 and w_c as sketched in Fig. 2, which is taken as an approximation of a more complex softening as suggested by the dashed line.

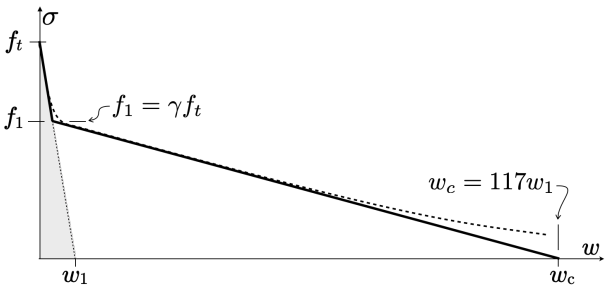

Figure 2: Bilinear softening considered in this work.

To account for the effect of fibre-bridging, we consider softening tails which are much longer than for ordinary concrete, and, to reduce the number of degrees of freedom, consider the subset of bilinear curves in which $w_c = 117 w_1$.

Note This value is not totally arbitrary, it comes from considering the pullout of a bundle of rigid fibers of length l_f from a rigid half-space subjected only to mutual constant drag shear force per unit length of fiber, assuming a uniform distribution of initial pullout lengths; after a few simplifications it turns out that the value of w_c is $\approx l_f/4$ which, for a

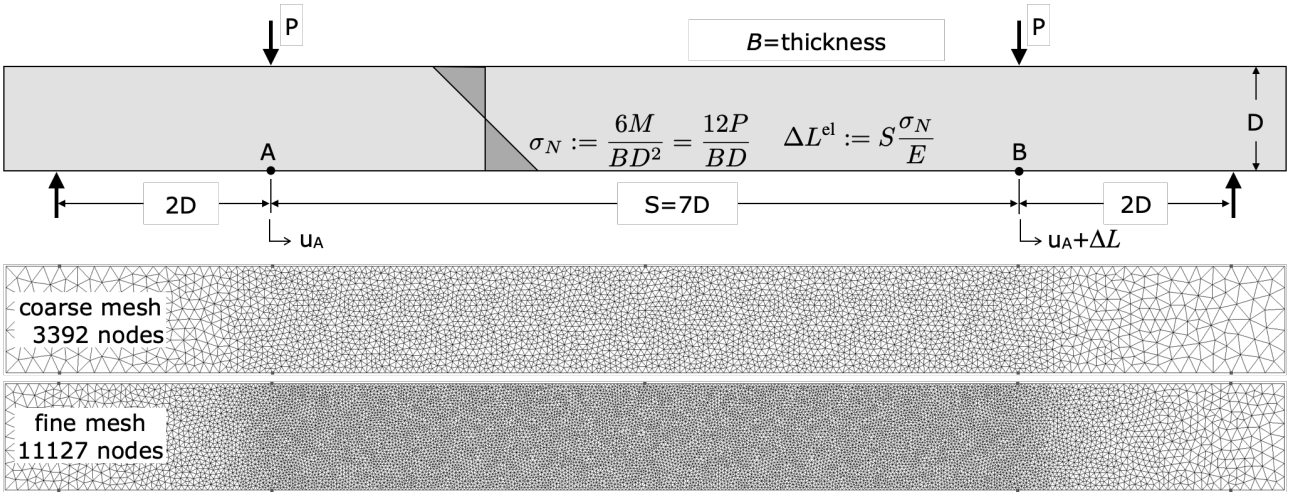

Figure 1: Beam geometry and meshes (adapted from [4].

well known industrial UHPFRC is 3.5 mm; assuming further a value of $w_1 \approx 30\,\mu$m for the matrix, we get $w_c/w_1 = 116.7$ which we round to 117.

The computations we analize in this paper have been carried for two shapes of softening curves, corresponding to two values of $\gamma := f_1/f_t$, namely $\gamma = 0.4$ and $\gamma = 0.7$, and for each of those softening curves, computations have been carried out for two very different values of the structural toughness number, namely $\ell_2/D = 1$ and $\ell_2/D = 16$. Only one of the four resulting cases was previously analyzed in [4], namely, the case with $\gamma = 0.7$ and $\ell_2/D = 1.0$.

The computations have been carried out using the finite element method using constant strain elements with an embedded cohesive crack as described in detail elsewhere [6, 14, 15] and implemented in the program COFE (Continuum Oriented Finite Elements).

All the computations have been carried out under control of the relative horizontal displacement of points A and B, which is denoted as ΔL in the following (see Fig. 1).

4 RESULTS

The essential numerical results are the dimensionless versions of the generalized load-displacement curves and the crack patterns. In particular, Fig. 3 shows the plots of the dimensionless *nominal stress* σ_N in the central span versus the *inelastic elongation* ΔL^{in} for the various cases and meshes envisaged, where the inelastic elongation is defined as

$$\Delta L^{in} := \Delta L - \Delta L^{el}$$

and ΔL^{el} is the *nominal elastic elongation* defined, together with σ_N, in Fig. 1. The first thing to note from these graphs is that a spurious mesh dependency does not seem to exist since the results for the two meshes are close to each other except, maybe, when local instabilities occur due to successive growth of new cracks. Indeed, severe instabilities occur in the diagrams for the most brittle material ($\gamma = 0.4$), which are indicated by dashed lines to make clear that the transition from one equilibrium state to the next is not an equilibrium path; such behavior is due to the fact that the control gauge length used in the simulations is too long for the control to be effective when one of the various growing cracks gets suddenly dominant, similar to what is observed in testing when the testing machine is not rigid enough or the control system not fast enough (although in the numerical computation no dynamic effects are involved).

Diagrams for the tougher material ($\gamma = 0.7$) show that hardening occurs in for the two extreme cases of structural toughness number studied here. Since in [4] it was found that this softening displays hardening also for the intermediate values $\ell_2/D = 2, 4, 8$ we can conclude that it hardens in the whole range of values of ℓ_2/D in the interval $[1, 16]$. Note, however than the curves for the upper limit of the interval are

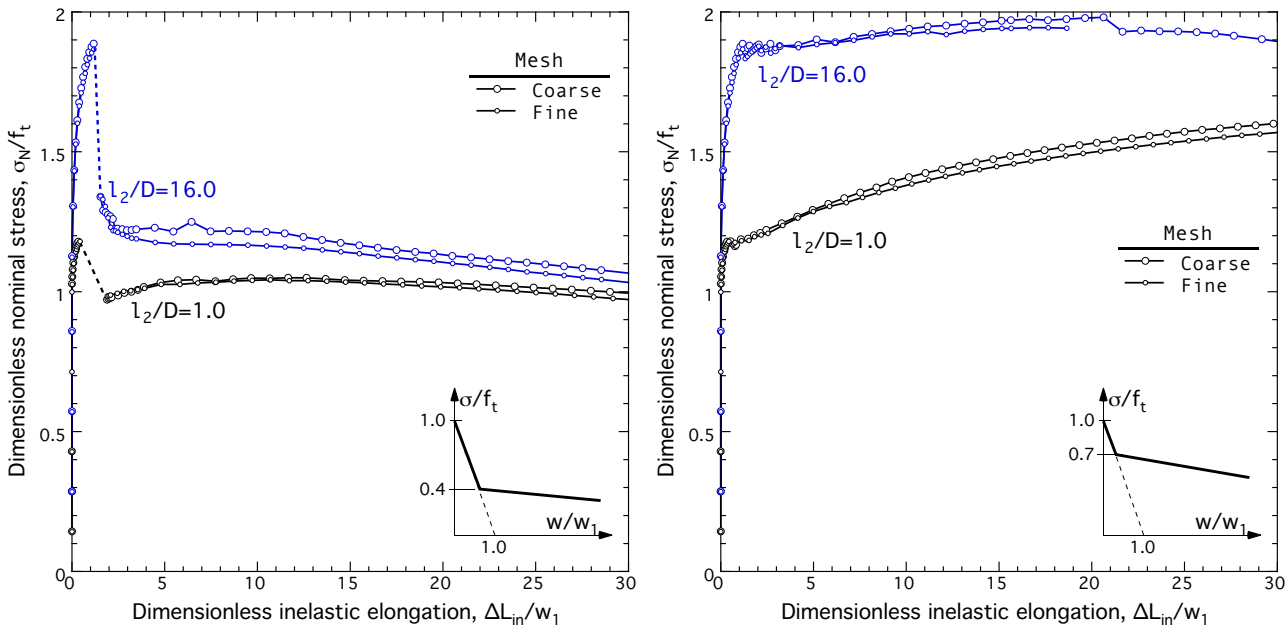

Figure 3: Dimensionless plots of nominal stress σ_N vs. inelastic elongation ΔL^{in}, for the two meshes and the two structural initial toughnesses studied in this paper: for the more brittle material (left) and the tougher material (right).

flatter than for the initial limit and we may suspect that for larger values of ℓ_2/D the hardening can turn into softening as hypothesized in [4] based on the behavior for the rigid-softening limit ($\ell_2/D \to \infty$). Further simulations may settle this point.

An expanded view of the curves around the first relative maximum reveals that previous to reaching that point the behavior is independent of the value of γ, as shown in Fig. 4. This is due to the fact that, for the range of values analyzed, all the cracks in the beam are still on the initial linear softening. This will become even more evident later in the presentation.

To continue the presentation of results, Figures 5-8 collect the evolution of crack patterns by means of a sequence of snapshots at selected steps for each of the cases considered. Figures 5-6 correspond to the most brittle material ($\gamma = 0.4$) and Figs. 7-8 to the toughest one ($\gamma = 0.7$). For each case, the selected steps are identified by heavy red circles on a curve of (dimensionless) σ_N versus ΔL^{in} curve located at the top of each figure. Each selected spot is identified by a letter; lower case letters correspond to points up to the first peak, while uppercase letters correspond to points after that peak.

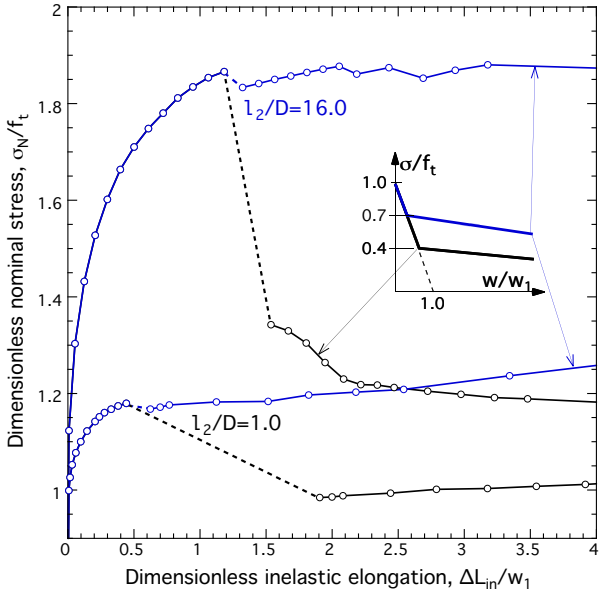

Figure 4: Response curves before and around the first relative maximum for the finest mesh.

Figures 5-6 for the most brittle material are very similar, although the second is easier to follow because multiple cracking is more visible. Cracking starts in the elements near the bottom line of the central span soon after σ_N exceeds the tensile strength f_t as in pattern a in both figures. As loading proceeds, some cracks grow faster and wider than the others and the pattern becomes sparser up to the first peak load (pattern f in Fig. 5, and pattern h in Fig. 6). In

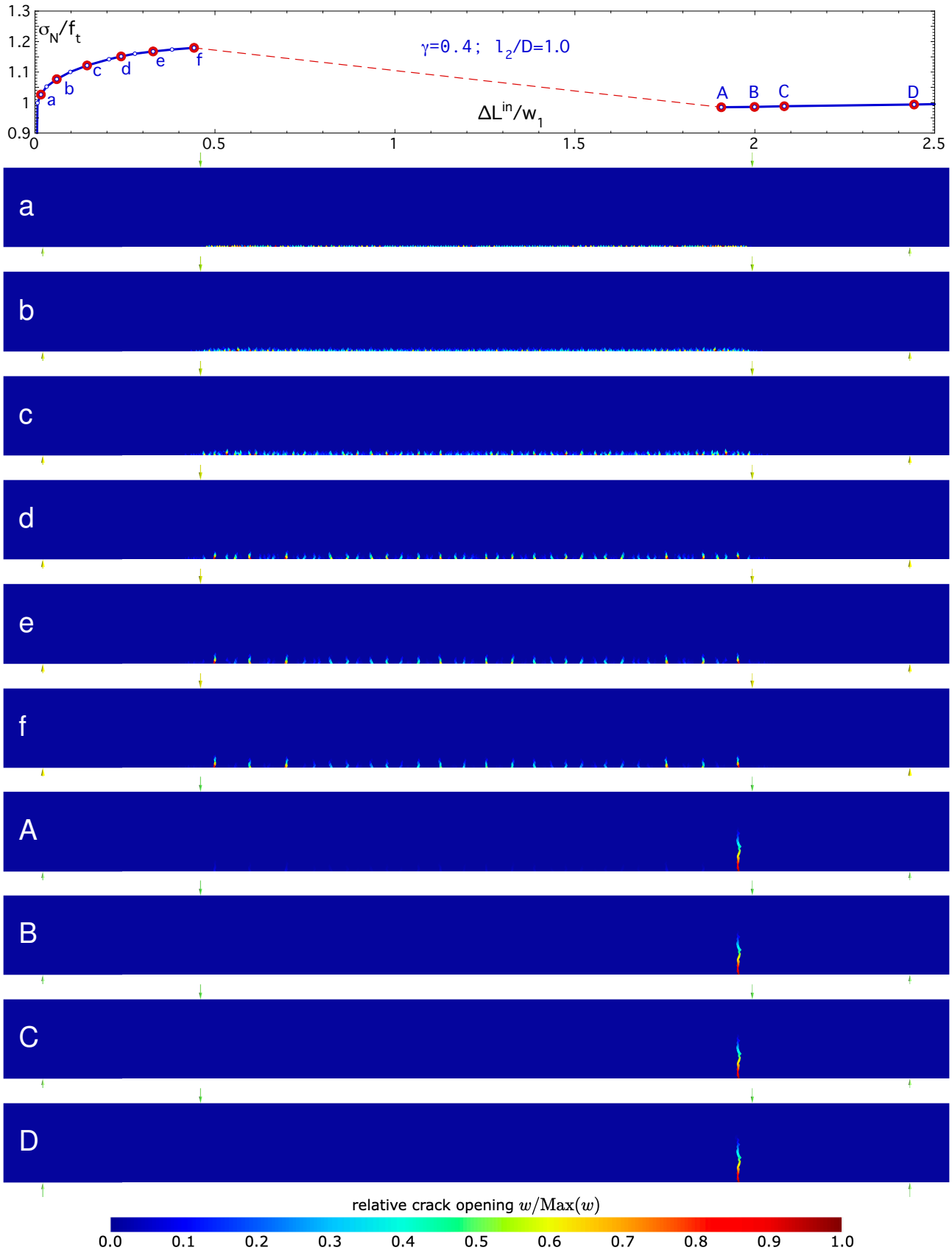

Figure 5: Crack pattern evolution for $\gamma = 0.4$ and $\ell_2/D = 1.0$.

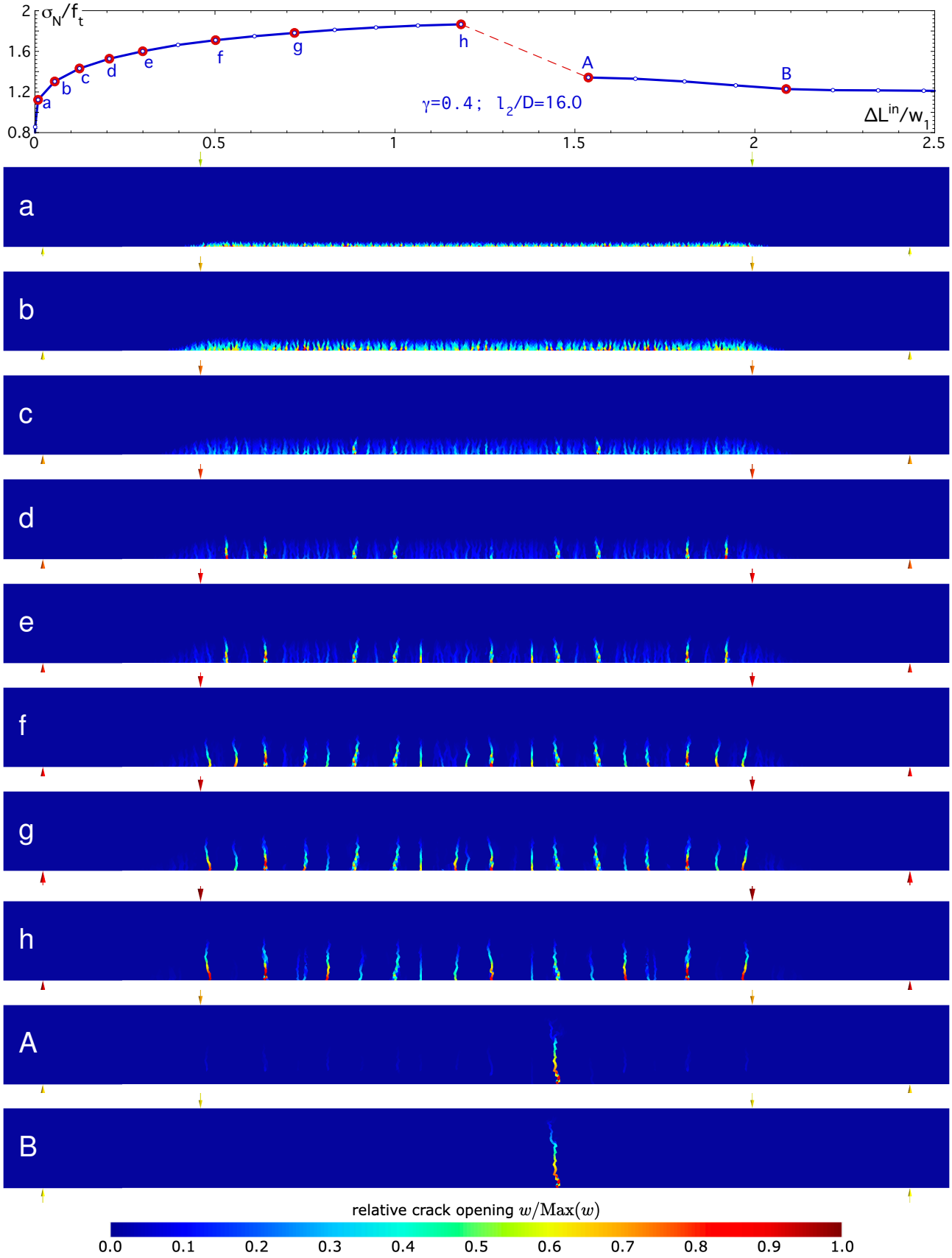

Figure 6: Crack pattern evolution for $\gamma = 0.4$ and $\ell_2/D = 16.0$.

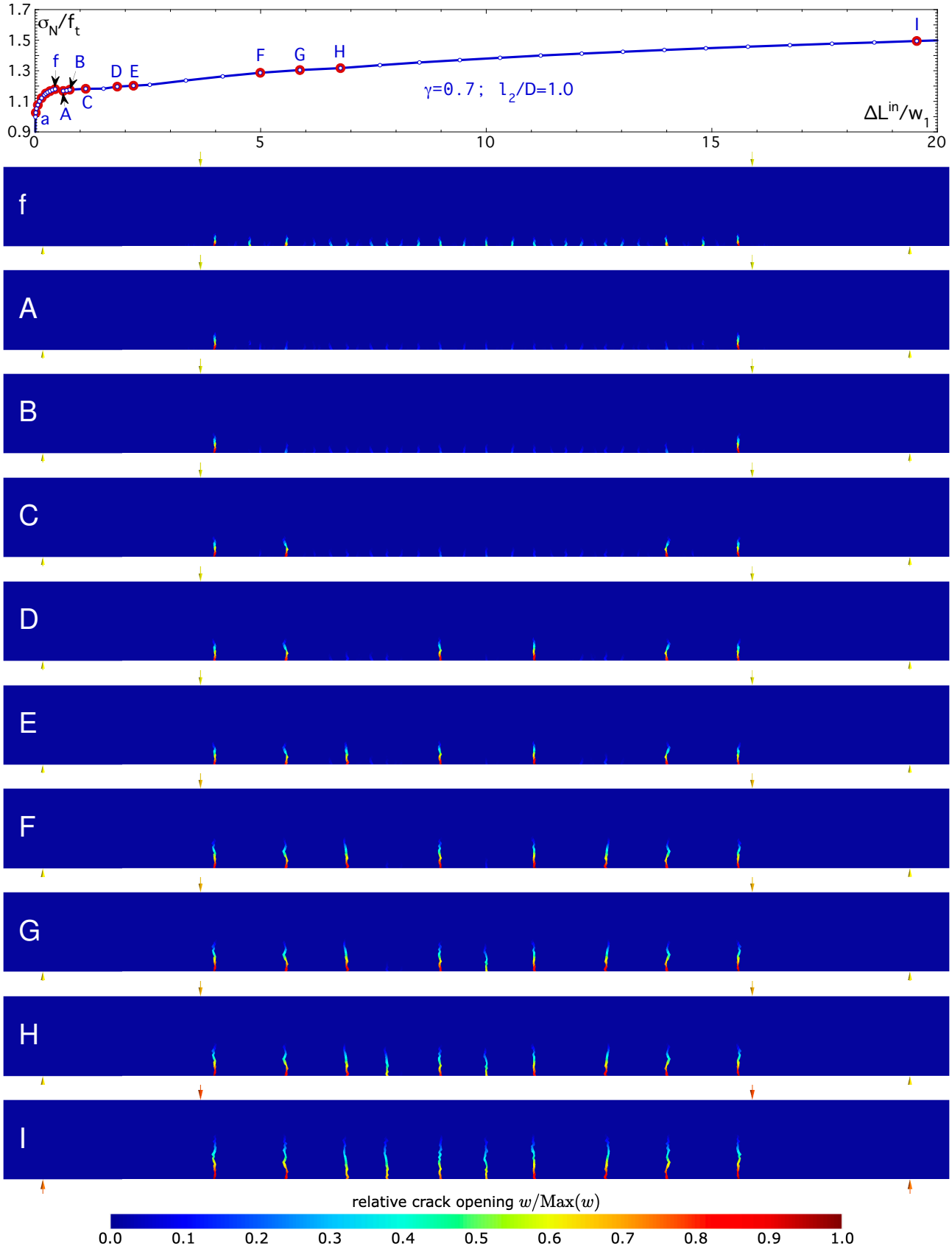

Figure 7: Crack pattern evolution for $\gamma = 0.7$ and $\ell_2/D = 1.0$.

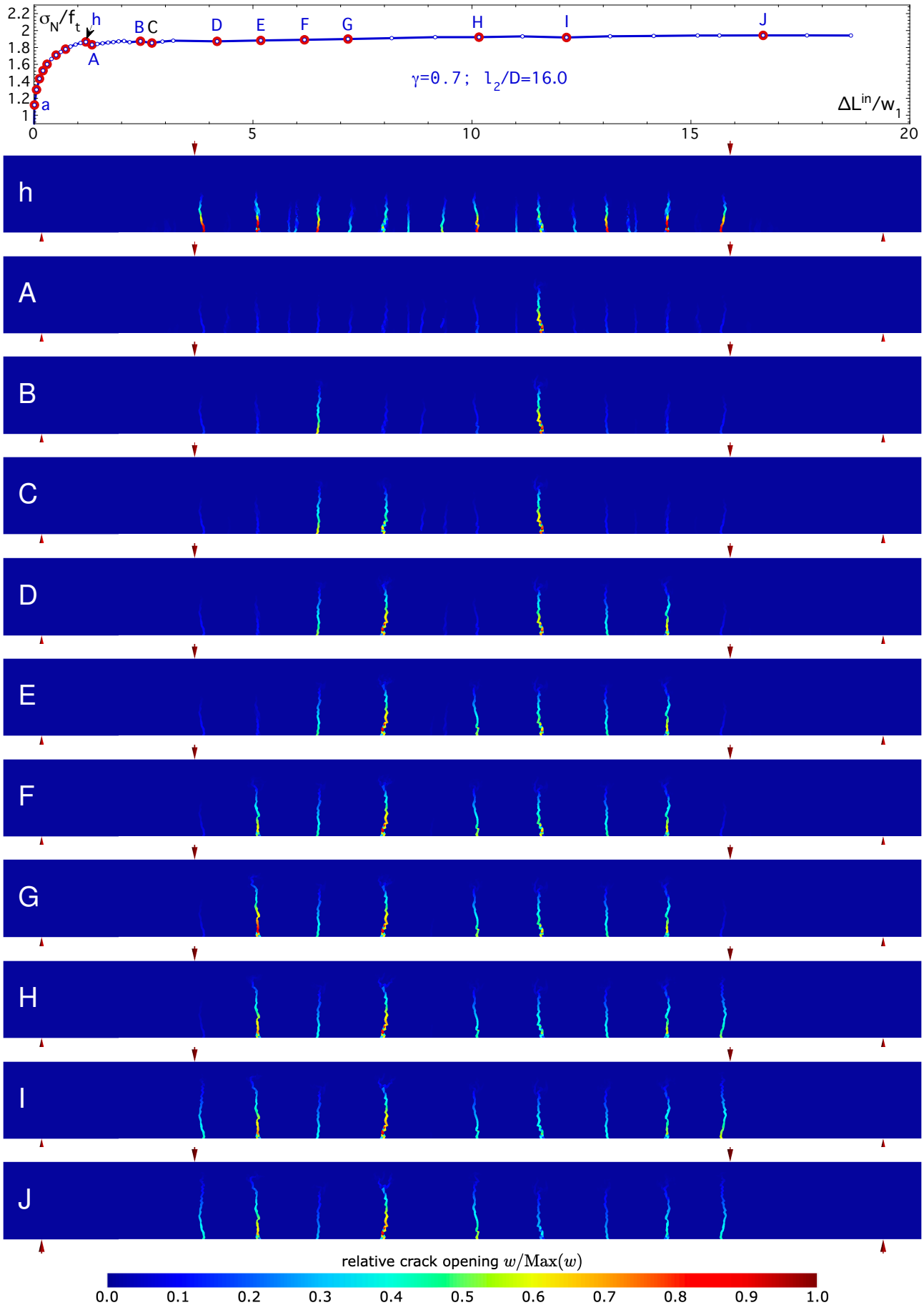

Figure 8: Crack pattern evolution for $\gamma = 0.7$ and $\ell_2/D = 16.0$.

the next computational step after the peak, pattern A, a single crack becomes dominant in both cases while the others fade out, a pattern that is preserved up to the termination of the computation for these two cases.

Going next to the patterns for the toughest material, the behavior is subtly different for the low and large values of ℓ_2/D, and so we comment them independently. For the case in Fig. 7, the patterns of the steps up to the first peak are identical to those in Fig. 5, and so we start the sequence at pattern f and see that in the step just after it, pattern A, two cracks become dominant, as well as in point B, but in C the cracks become four, six in D and the number of cracks keeps increasing up to ten at point H, and from this point on the crack pattern remains stable up to I and further up to the termination of the computations for ΔL^{in} well over $50w_1$.

For the case in Fig. 8, the patterns of the steps up to the first peak are identical to those in Fig. 6, and so we start the sequence at pattern h and see that in the step just after it, pattern A, there is a single dominant crack, although other cracks are visible as filaments of slightly lighter shadows of blues that the dark-blue background that corresponds uncracked material. At this point it becomes necessary to specify that the coloring of the elements is done relative to the maximum value of the crack opening in the corresponding step, according to the color scale at the bottom of each figure. Thus we see that in the following point B one of the preexisting, scarcely open cracks, starts to open again into the light-blue range, then in C a third crack becomes clearly visible and so on the number of cracks increases up to eight in H, nine in I and keeps the same in J, although the dominant crack (the fourth counting from the left) keeps its colors while the others seem to slightly fade out. Unfortunately no convergence was achieved for the two steps following J and so this is the last valid computation in the series.

To finish the presentation and discussion of results, we give a compact view of the maximum crack opening found in the specimen at the end of each step by placing it in a cohesive stress versus crack opening diagram. The resulting plots are shown in Figs. 9 and 10 in which the dashed lines mark the jumps from the point corresponding to first local peak, which is always located on the first linear branch of the the softening, to the next equilibrium point, which is always located on the second branch of the softening curve.

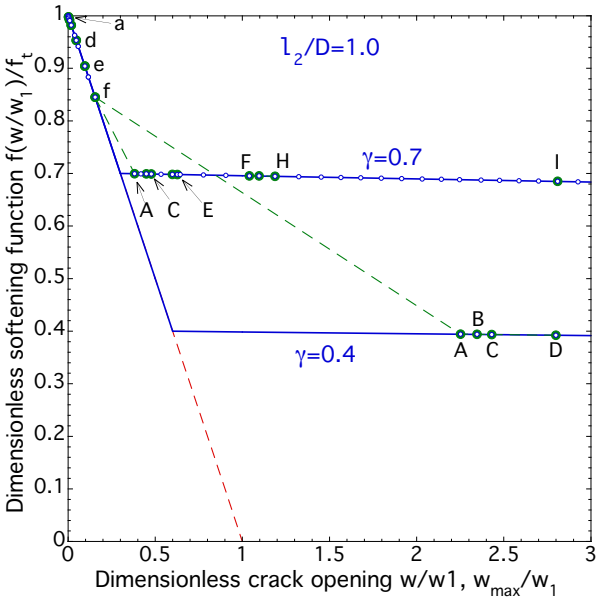

Figure 9: Position on the softening curves of the points corresponding to the maximum crack openings at each of the steps in Figs. 5 and 7.

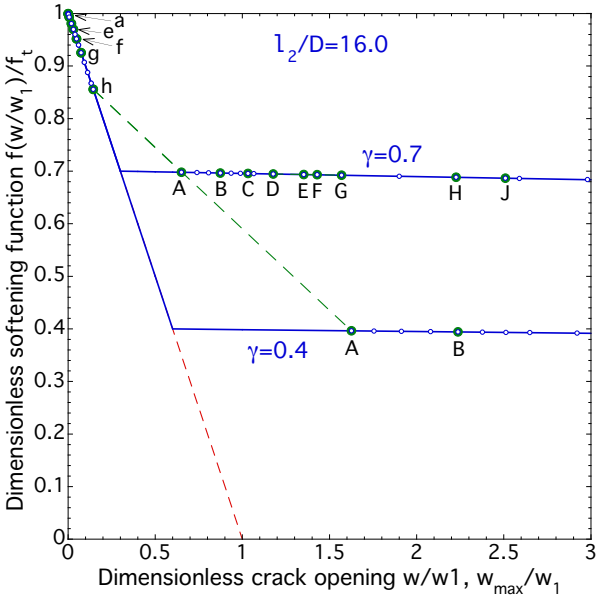

Figure 10: Position on the softening curves of the points corresponding to the maximum crack openings at each of the steps in Figs. 6 and 8.

These figures make blatantly clear that up to the first peak (lower-case letters) the points lie on the initial softening branch.

5 FINAL REMARKS

The results just reported are consistent with the conclusions reached in [4], and, in addition to broadening the spectrum of the analyses by adding a material with a lower toughness $\gamma = 0.4$ and getting results for a structural toughness number ℓ_2/f_t never investigated before, they bring insight on how the crack patterns evolve since the initiation of cracking soon after the nominal stress exceeds the tensile strength.

Indeed, the progression is roughly similar: it starts with a great-many of tiny cracks that grow or fade-out as load grows in a increasingly deeper and sparser array of many cracks that, at a certain point, gets unstable and only one or two cracks survive; then, depending on the combination of material and structural toughnesses, either one single crack grows under softening, or further cracks open under hardening.

The foregoing is valid for the range of toughnesses used so far, and may be expected to hold for lower material toughnesses down to $\gamma = 0$ (linear softening), but it is obvious that hardening cannot hold forever, and that a second peak load must exist followed by softening down to full fracture. The problem is that in most cases we cannot reach this stage because of computational limitations of two types: first because when the crack tips get close to the upper free surface, to within a distance of one or two elements, a spurious hardening occurs due to excessive gradients, and second because with the algorithm currently used in our computations the convergence rate decreases appreciably with the number of cracked elements and cannot cope with many simultaneous cracks growing in a very fine mesh.

One relevant issue concerns the unstable steps found in the foregoing computations, especially those occurring at the first load peak when going from many-crack to single-crack, but also those that occur when a new crack suddenly appears in the pattern. Although both the initial and the final states satisfy equilibrium (to within numerical tolerance), it is not obvious that the reached final state do coincide with the state the system would reach if the process were under full control. A better control system keeping the jumps within 'reasonable' limits would be required and work is in progress to develop it.

A final caveat regarding the reliability of the crack patterns: previous works [6] showed that the *details* of the crack patterns *do* depend on the mesh and the step size, but the global, average values are thought to be reasonably approximate. Quoting from [6]:

> "Of course, the localization is triggered by the small inhomogeneities induced by the mesh itself (which is a spurious, purely numerical inhomogeneity, not a material one). But there seems to be a sufficiently rich set of locally stable configurations for the calculations to be meaningful at large."

ACKNOWLEDGMENTS

The authors gratefully acknowledge the financial support received for this work under grant PID2021-125553NB-I00 from MCIN/AEI/10.13039/501100011033 and FEDER, UE.

REFERENCES

[1] AFGC, 2013. *Ultra High Performance Fibre-Reinforced Concretes: Recommendations.*, AFGC, june 2013, revised edition.

[2] NF-P18-470, 2016. *Concrete – Ultra-high performance fibre-reinforced concrete – Specifications, performance, production and conformity.*, AFNOR.

[3] NF-P18-710, 2016. *National addition to Eurocode 2 – Design of concrete structures: specifique rules for ultra-high performance fibre-reinforced concrete (UHPFRC)*, AFNOR.

[4] Planas, J., Sanz, B., and Sancho, J.M., 2021. Numerical analysis of size-effect in

UHPFRC beams subjected to wide-span four-point bending. *Revista de Mecánica de la Fractura* **1**:149–154.

[5] Sanz, B., Planas, J., and Sancho, J.M., 2013. An experimental and numerical study of the pattern of cracking of concrete due to steel reinforcement corrosion. *Engineering Fracture Mechanics* **114**:26–41.

[6] Planas, J., Sanz, B., and Sancho, J.M., 2016. Transition from smeared to localized cracking in macro-defect-free quasibrittle structures. *Procedia Structural Integrity* **2**:3676–3683.

[7] Wille, K., El-Tawil, S., and Naaman, A.E., 2014. Properties of strain hardening ultra high performance fiber reinforced concrete (uhp-frc) under direct tensile loading. *Cement and Concrete Composites* **48**:53–66.

[8] Hillerborg, A., Modéer, M., and Petersson, P.E., 1976. Analysis of crack formation and crack growth in concrete by means of fracture mechanics and finite elements. *Cement and Concrete Research* **6**:773–781.

[9] Elices, M. and Planas, J., 1989. Material models, chapter 3, in L. Elfgren (Ed.), *Fracture Mechanics of Concrete Structures*, pp. 16–66, Chapman & Hall, London.

[10] Bažant, Z.P. and Planas, J., 1998. *Fracture and Size Effect in Concrete and Other Quasibrittle Materials*, CRC Press, Boca Raton, FL.

[11] Elices, M., Guinea, G.V., Gómez, J., and Planas, J., 2002. The cohesive zone model: advantages, limitations and challenges. *Engineering Fracture Mechanics* **69**:137–163.

[12] Planas, J., Elices, M., Guinea, G.V., Gomez, F.J., Cendon, D.A., and Arbilla, I., 2003. Generalizations and specializations of cohesive crack models. *Engineering Fracture Mechanics* **70**:1759–1776.

[13] Kim, D.J., Naaman, A.E., and El-Tawil, S., 2010. Correlation between tensile and bending behavior of frc composites with scale effect, in e.a. B. H. Oh (Ed.), *Fracture Mechanics of Concrete and Concrete Structures - High Performance, Fiber Reinforced Concrete, Special Loadings and Structural Applications*, Korea Concrete Institute.

[14] Planas, J., Sanz, B., and Sancho, J.M., 2020. Vectorial stress-separation laws for cohesive cracking: in concrete and other quasibrittle materials. *International Journal of Fracture* **223**:77–92.

[15] Sancho, J.M., Planas, J., Cendon, D.A., Reyes, E., and Galvez, J.C., 2007. An embedded crack model for finite element analysis of concrete fracture. *Engineering Fracture Mechanics* **74**:75–86.

[16] Geuzaine, C. and Remacle, J.F., 2009. Gmsh: A 3-d finite element mesh generator with built-in pre- and post-processing facilities. *International Journal for Numerical Methods in Engineering* **79**:1309–1331.